Water Research 200 (2021) 117221

Contents lists available at ScienceDirect

Water Research

journal homepage: www.elsevier.com/locate/watres

Reductive defluorination of Perfluorooctanesulfonic acid (PFOS) by hydrated electrons generated upon UV irradiation of 3-Indole-acetic-acid in 12-Aminolauric-Modified montmorillonite

Alex Kugler[a], Hailiang Dong[a,*], Chen Li[b], Cheng Gu[b], Charles E. Schaefer[c], Youn Jeong Choi[d], Danielle Tran[c], Morgan Spraul[c], Christopher P. Higgins[d]

[a] Department of Geology and Environmental Earth Sciences, Miami University, Oxford, OH, United States
[b] State Key Laboratory of Pollution Control and Resource Reuse, School of the Environment, Nanjing University, Nanjing 210023, PR China
[c] CDM Smith, Edison, New Jersey, United States
[d] Department of Civil and Environmental Engineering, Colorado School of Mines, United States

ARTICLE INFO

Article history:
Received 21 January 2021
Revised 23 April 2021
Accepted 3 May 2021
Available online 9 May 2021

Keywords:
ALA
degradation
IAA
montmorillonite
PFOS
sorption

ABSTRACT

Per-and poly-fluoroalkyl substances (PFASs) are a class of persistent compounds that are resistant to degradation. Here we developed an effective method of degrading perfluorooctanesulfonate (PFOS) by hydrated electrons (e_{aq}^-) that are generated from 3-indole-acetic-acid (IAA) upon UV irradiation. The method takes advantage of spatial proximity of IAA and PFOS by their co-sorption to an organic polymer, 12-aminolauric acid (ALA), which was pre-intercalated into the interlayer space of an expandable clay mineral, montmorillonite. The interlayer spacing of this clay nanocomposite is greatly expanded relative to unmodified montmorillonite. The maximum adsorption capacity of IAA and PFOS is 168 and 1550 mmol/kg, respectively. This process achieved 40–70% defluorination of a 10 ppm PFOS solution at neutral pH in a 325 mL vessel. The presence of bicarbonate and chloride ions, or natural groundwater showed a minimal impact on PFOS degradation. Based on identification of prominent degradation products, a degradation pathway is proposed, where the primary degradation process is breakage of the C-F bonds (with fluorine replaced by hydrogen), with some cleavage of the C–C bond. This approach provides an alternative for treating concentrated PFAS solutions under ambient conditions.

1. Introduction

Per- and polyfluoroalkyl substances (PFASs) are a class of synthetic chemical compounds with surfactant properties. These compounds are useful in various industrial applications such as textiles, carpet manufacturing, food packaging, leather treatment, and fire-fighting foam (Houtz et al., 2013; Sznajder-Katarzyńska et al., 2019). These prolific uses of PFASs are largely ascribed to the strength of the carbon - fluorine bond, which requires 485 kJ/mol to break (O'Hagan 2008). A subclass of PFASs, perfluoroalkyl acids (PFAAs), are thermally stable and resistant to oxidation. Because of their widespread applications, PFAAs have made into the EPA's list of emerging contaminants. PFAAs are persistent and bio-accumulative, and have been shown to be environmentally hazardous and potentially carcinogenic (Cooke 2017; Sznajder-Katarzyńska et al., 2019). Due to its widespread occurrence and regulatory focus, perfluorooctanesulfonic acid (PFOS), a particular PFAA, has received much attention. While production in the United States has voluntarily been phased out since 2002, PFOS still exists as a legacy product (Cooke 2017). Thus, exposure to PFOS in the United States remains a concern.

Several technologies have recently been explored for the destructive defluorination of PFAAs, including photocatalytic (Chen et al., 2020; Tian et al., 2016), plasma (Lewis et al., 2020); and electrochemical (Schaefer et al., 2019; Wang et al., 2020) treatments. However, these methods often do not completely break down PFASs, and they either require expensive electrodes, use hazardous materials, or are energy-intensive. While ultrasonic degradation has achieved success in complete defluorination, the required frequency and power greatly limit the application of this method (Fernandez et al., 2016).

Photochemical methods used to defluorinate PFAAs often rely on hydrated electrons, as these are highly reactive (Cui et al., 2020). Hydroxyl radicals are ineffective for PFAAs, likely due to the high strength of the C-F bond (Javed et al., 2020). However, highly

* Corresponding author.
E-mail address: dongh@miamioh.edu (H. Dong).

https://doi.org/10.1016/j.watres.2021.117221
0043-1354/

reductive hydrated electrons can break the C-F bond (Bentel et al., 2019; Chen et al., 2020; Gu et al., 2020; Wang et al., 2020). While previous studies (Qu et al., 2014; Qu et al., 2010; Song et al., 2013) have used hydrated electrons, generated through photoionization of iodide or sulfite, for treatment of PFOA and PFOS, the large-scale application of this approach may be limited due to: 1) the toxicity of iodide and sulfite, and generation of elevated levels of undesirable byproducts (e.g., sulfate); 2) the difficulty of maintaining anoxic and high pH conditions that are required for the defluorination reaction, as both O_2 and protons can quickly consume hydrated electrons.

Recent studies (Gu et al., 2016; Gu et al., 2017a) have used hydrated electrons to degrade both PFOS and PFOA under partially oxic (dissolved oxygen, DO=5 mg/L) and alkaline pH (9.2) conditions. Loss of hydrated electrons from reaction with O_2 is partially compensated by a high production rate in a high photon flux UV/sulfite system. A more recent study has examined the effects of vacuum ultraviolet (VUV) at a pH of 12 (Bentel et al., 2020). However, sulfite and an alkaline condition (pH > 9) were still required in these systems. Other studies have adopted variations of UV systems to alleviate some of these requirements. Sun et al. (2018) used a combination of UV and nitrilotriacetic acid (NTA), which scavenged hydroxyl radicals and thereby minimized their reaction with hydrated electrons. While PFOS degradation was still sensitive to pH, it was less sensitive to O_2 level. Gu et al. (2020) observed photoreductive degradation of PFOS by UV irradiation in the presence of ethylenediaminetetraacetic acid (EDTA) over a range of pH (4–10) with the removal of O_2, but the degradation and defluorination efficiency of PFOS at acidic pH were much lower than at alkaline pH. In this process, EDTA served as a scavenger of hydroxyl radicals. However, EDTA is toxic (Oviedo and Rodríguez 2003). In addition, in treatment systems with complicated water chemistry containing organic matter, co-contaminants, and anions (such as bicarbonate/carbonate, sulfate, and nitrate), hydrated electrons can rapidly react with these species and further lower their efficiency towards PFAS degradation (Buxton et al., 1988; Gu et al., 2016; Gu et al., 2017b).

Tian et al. (2016) developed a novel approach through the use of an organic polymer, hexadecyltrimethylammonium bromide (HDTMA), that was intercalated into the interlayer region of a clay mineral montmorillonite. This HDTMA-montmorillonite nanocomposite was highly hydrophobic and even organophilic. PFOA/PFOS and 3-indole-acetic acid (IAA), a common component of natural organic matter in soils and sediments (Chen and Kenny 2007; Miura et al., 2011) and a source of hydrated electrons, were co-sorbed to HDTMA. Upon UV irradiation, hydrated electrons were generated from IAA to degrade adjacent PFOA/PFOS. The negatively charged planar surface of HDTMA-modified montmorillonite stabilized indole radical cations, consequently inhibiting their recombination with hydrated electrons. Nearly complete reductive defluorination of both PFOA and PFOS was achieved over a pH range of 3–11 and in air (Tian et al., 2016). The authors postulated that the interlayer region of montmorillonite prevented entry of protons and dissolved oxygen to consume hydrated electrons. A more recent study (Chen et al., 2020) reported a near complete defluorination of PFOA by hydrated electrons even without montmorillonite scaffold. This approach used positively-charged HDTMA to co-sorb negatively-charged PFOA and IAA to form self-assembled micelles, which increased the degradation efficiency of PFOA due to the spatial proximity between hydrated electrons and PFOA (Chen et al., 2020).

Despite these encouraging results, this approach has a few limitations. It is well-known that HDTMA is toxic and antibacterial, even when it is intercalated into the interlayer region of montmorillonite (Boyd et al., 1988). Additionally, the maximum sorption capacity of HDTMA-montmorillonite is lower than other alternatives such as resins (Deng et al., 2010; Yu et al., 2009; Zaggia et al., 2016; Zhang et al., 2019). For these reasons, a more environmentally friendly and highly adsorbing material is desirable. In addition, while this clay nanocomposite-based approach has been shown for PFOA degradation (Tian et al., 2016), the pathway for PFOS degradation and intermediate product formation has not been identified. Some intermediate degradation products may be more toxic than the parent compound (Brendel et al., 2018; Kabadi et al., 2020; Rice et al., 2020). Finally, the effects of natural organic matter, co-contaminants, and competing anions such as nitrate, and bicarbonate on PFOS degradation are currently unknown. A potential replacement, which overcomes many of the limitations of HDTMA, is 12-Aminolauric acid [ALA; $NH_2(CH_2)_{11}COOH$)]. ALA is a saturated omega fatty acid with a 12-carbon atom chain, possessing both amino and carboxylic groups. It has many properties of medium-chain fatty acids. It is nontoxic and readily found in many edible plants (Liu et al., 2013). ALA is a bacterial metabolite (Wilding et al., 2015), and can be readily intercalated into the expandable clay interlayer when protonated (Zeng et al., 2016).

The objective of this study was to develop a technique to effectively degrade PFASs under specific conditions. PFOS was selected as a model compound due to its prevalence and high recalcitrance. To achieve a high rate and extent of PFOS degradation, IAA was selected because it has a high efficiency of emitting hydrated electrons upon UV irradiation (a 254 nm monochromatic source) (Tian et al., 2016). ALA was pre-intercalated into the interlayer region of montmorillonite. Sorption isotherms of IAA and PFOS onto ALA-modified montmorillonite were determined. The rate and extent of PFOS degradation and defluorination were subsequently determined, along with identification of transformation products of PFOS degradation. The effects of competing anions and natural groundwater were evaluated so that this technology could be evaluated for *in* or *ex situ* application to contaminated water. This study develops a PFOS degradation technology, which potentially can be used to remediate contaminated water without hazardous chemical additions.

2. Materials and methods

2.1. Chemicals

All chemicals used were of laboratory grade or higher and procured from Fisher Scientific unless specified elsewhere. HDTMA bromide, and PFOS (CAS Number 1763–23–1) were purchased from Sigma-Aldrich. Water, methanol, and ammonium acetate used for cleaning and mobile phases were purchased from Fisher as LC/MS grade.

2.2. Synthesis of organoclay nano-composites

Montmorillonite SWy-3 was procured from the Source Clays Repository of the Clay Minerals Society (West Lafayette, IN). Bulk SWy-3 was ground and 0.02–0.5 μm size fraction was separated by repeated suspension and centrifugation. ALA-intercalated montmorillonite nanocomposite was synthesized according to a previous method (Zeng et al., 2016). The HDTMA-montmorillonite nanocomposite was prepared as described previously (Boyd et al., 1988). The detailed method for clay separation and synthesis of ALA- and HDTMA-intercalated montmorillonite nanocomposites is described in Section 1 of the Supporting Information (SI). To confirm intercalation of ALA into the montmorillonite interlayer, powder X-ray diffraction (XRD) analysis was performed for SWy-3, HDTMA-modified SWy-3, and ALA-modified SWy-3 (SI Section 2). Additional characterization was not carried out, because our previous study already characterized ALA-intercalated clay nanocom-

posite (Zeng et al., 2016) including XRD, Fourier transform infrared spectroscopy (FTIR), and total organic carbon (TOC) analysis.

2.3. Batch sorption experiments of IAA, F^-, and PFOS

Batch equilibrium experiments were carried out to determine sorption of IAA, F^-, and PFOS onto SWy-3 clay and organoclay nanocomposites. The fluoride sorption experiment was performed to account for any possible loss of aqueous F^- that may be released from PFOS defluorination. SWy-3 clay and organoclay nanocomposites were kept at a concentration of 2.2 g/L. For time course kinetic experiments, initial concentrations of 1 mM, 1 mM, and 1 ppm were used for IAA, PFOS, and F sorption, respectively. For sorption isotherm experiments, the initial concentrations of IAA and PFOS ranged from 0.05 mM to 2.25 mM, and from 0 to 20 mM, respectively. For both types of experiments, the adsorbed amounts of IAA and PFOS were calculated by the difference in aqueous concentration between the initial and the final time points. All sorption experiments were carried out in duplicate. The detailed methods for these sorption experiments are described in SI Section S3.

2.4. IAA, F^-, and PFOS analyses from sorption experiments

IAA concentration was analyzed spectrophotometrically using a method modified after Tang and Bonner (1948) using a Thermofisher Genesys 10vis spectrophotometer (Waltham, MA). For high throughput analysis, F^- concentration was analyzed using the SPADNS colorimetric method, which is based on the reaction between fluoride and a zirconium-dye lake (Marier and Rose 1966). Fluoride concentration was also periodically checked using ion chromatography (IC). These two methods compared favorably with no significant difference.

For high concentration sorption experiments ($>$ 3 mM), PFOS concentration was determined using an HPLC system. For low concentration sorption experiments ($<$ 3 mM), samples were analyzed commercially at Eurofins laboratory (Sacramento, Ca) (Shoemaker 2018). These methods are described in SI Section S4.

2.5. Experimental setup of PFOS degradation

The PFOS degradation experiments were conducted in a photochemical reactor (model XPA-7, Xujiang Electromechanical Inc., Nanjing, China) equipped with an internal quartz photoreactor (height = 400 mm; internal diameter = 40 mm, volume = 325 mL). The UV source was a low-pressure mercury lamp (Philips; 254 nm, 36 W), which was fully immersed into the reaction solution. The light intensity at the surface of the sheath was 4.5 mW cm^{-2} (Tian et al., 2016). At the beginning of the experiment, SWy-3 and ALA-SWy-3 were pre-loaded into the reactor, to which IAA and PFOS were subsequently added. The initial concentrations of PFOS, IAA, and clays were 10 mg/L, 1 mM, and 2.2 g/L, respectively, in 18.2 Mohm•cm water. A high PFOS concentration of 10 mg/L was selected to facilitate F detection and was relevant to PFAS-concentrated wastewater. The pH was adjusted to 7 using 1 N HCl or NaOH. The PFOS, IAA, and clay suspensions were homogenized with a stir plate. The degradation experiment was initiated when the UV lamp was turned on. The reaction vessel was kept at ambient temperature using a circulating water bath. Various controls were run along with samples, including no-UV source, no IAA, and no clay. Duplicate experiments were conducted. Sampling times were pre-determined according to a previous study (Tian et al., 2016), at which points, subsamples of 5 mL in volume were collected from the reactor using a transfer pipette. The pH remained nearly neutral throughout the experiment.

In a separate experiment to maximize PFOS degradation, a high clay concentration (5 g/L) was used. The initial mixture of PFOS, clay, and IAA were allowed to mix overnight to achieve maximum sorption. At the beginning and over the course of the experiment, additional IAA was spiked three times (0, 3, and 6 h, 1 mM each time) to ensure adequate supply of hydrated electrons, while without disturbing the experimental setup.

To determine the potential effects of competing anions on PFOS degradation (Cheng et al., 2010; Schaefer et al., 2019), degradation experiments were repeated in the presence of 0–1 mM sodium bicarbonate or sodium nitrate. Degradation experiments were also performed in natural groundwater (procured from CDM Smith, see Table S1 for water chemistry). In the groundwater experiment, 10 ppm PFOS was spiked into the groundwater in the presence of 1 mM IAA and 2.2 g/L of clay. The pH of the groundwater remained at ~6.5 throughout the experiment.

2.6. Analysis of PFOS and degradation products

Analysis of PFOS and its transformation products in aqueous solution required a high mass resolution, low detection limit method. Thus, these analyses were performed on a LC ultra-high pressure liquid chromatography (UHPLC) system. Data were acquired on a Sciex X500R Quadrupole Time-of-Flight Mass Spectrometer (QToF/MS) system SWATH® in Data-Independent Acquisition mode. The data were processed via Sciex OS software (ver 1.6.1) for quantification of target compounds with standards. Concerning the suspect compound analysis, a compiled list of candidate intermediates was screened using Sciex OS. Non-target analysis was conducted using Masterview (ver 1.3.1) for the extraction of peaks from the SWATH full scanned data and for statistical data analyses, including principal components analysis and log fold change versus p-value plot, shown as a volcano plot (Figure S1). Confidence of compounds in the list for suspect analysis and the created list by Masterview were identified from mass accuracy (mass error $<$ 5 mg/L), isotopic pattern from molecular formula (% difference isotope ratio $<$ 20%), and MS/MS library confirmation.

3. Results

3.1. Characterization of organo-clay nanocomposites

ALA and HDTLA intercalation increased the interlayer spacing of SWy-3 from 12.4 to 17.0 Å and from 12.4 to 13.2, respectively (Fig. 2, Table S2). Although the amount of ALA intercalated into the interlayer of SWy-3 was only 4 times cation exchange capacity (CEC), the interlayer spacing was expanded to a similar level as that achieved by much higher amounts of ALA, at least an order of magnitude higher than the amount used in this study (Pagtalunan et al., 2018). Between ALA and HDTMA, ALA expanded the layer spacing to a higher extent. Our previous study based on XRD, FTIR, and TOC analyses confirmed that intercalated ALA formed chemical bonds with clay mineral (Zeng et al., 2016).

3.2. Sorption experiments

Kinetic sorption experiments (Figure S3) demonstrated that IAA sorption to ALA-SWy-3 occurred quickly, with equilibrium attained within approximately 2 h. There was a negligible loss of IAA to glassware (i.e., no clay) and little sorption to unmodified SWy-3. The level of IAA sorption was similar between ALA-modified (Figure S3) and HDTMA-modified SWy-3 (Tian et al., 2016).

Rapid sorption of PFOS to ALA-SWy-3 was also observed (Figure S4), reaching equilibrium in approximately 5 h. In comparison, the rate and extent of PFOS sorption to SWy-3 were much lower. There was no measurable loss of aqueous PFOS in the absence of clay. Fluoride showed no measurable adsorption (Figure S5).

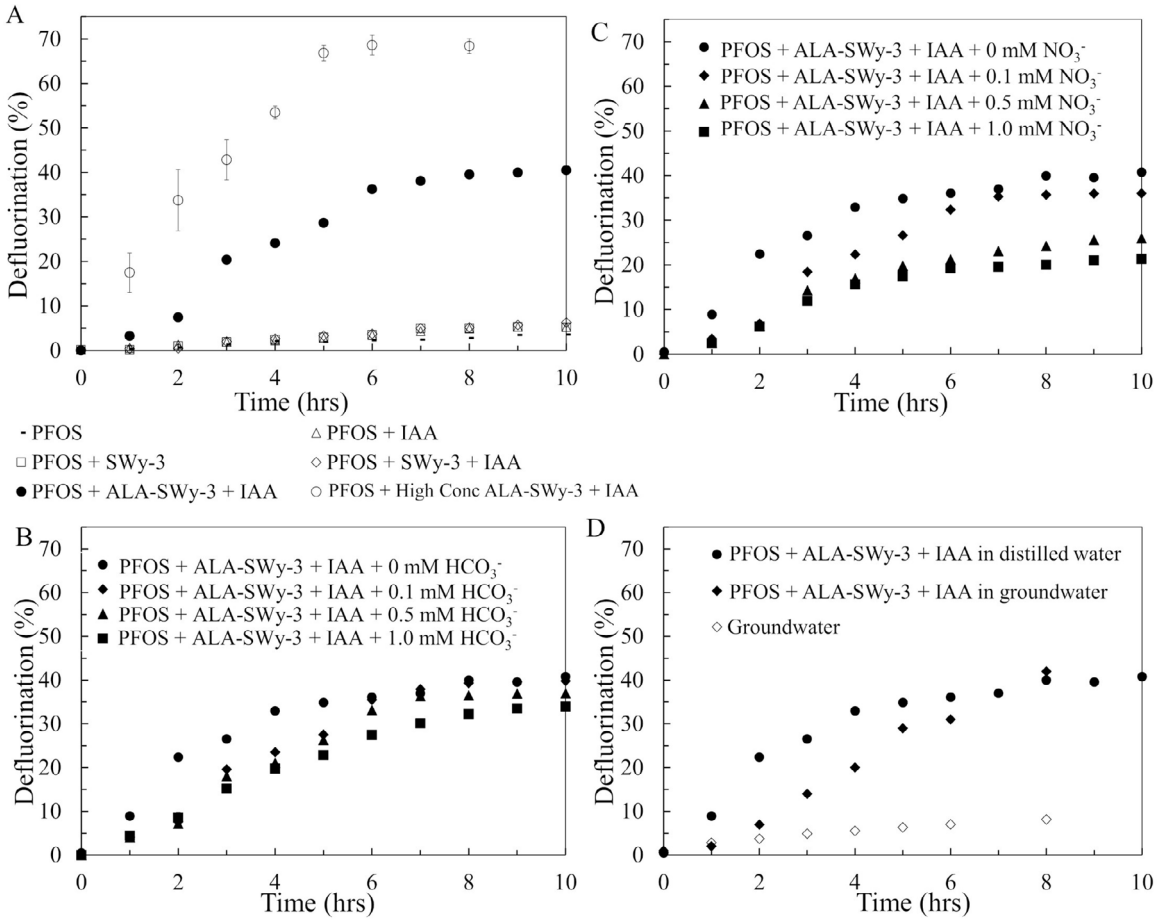

Fig. 1. Fluoride generation from PFOS degradation. All starting concentrations of PFOS were 10 ppm, all IAA concentrations were 1 mM, and all clay concentrations were 2.2 g/L except the red points, labeled as high concentration ALA-SWy-3 which was 5 g/L and IAA was added at 0, 3 and 6 h. A) ALA-SWy-3 yielded the highest amount of F, but SWy-3 showed a negligible amount of fluoride generation. Limited amounts of fluoride (<5%) were generated from PFOS with UV only, in the presence of IAA and SWy-3 alone, or in their combination. B) Different concentrations of bicarbonate anion showed an increasing interference as its concentration increases, however the interference even at 1 mM was small. C) Nitrate concentrations ranging from 0 to 1 mM showed a significant inhibition, with the extent of inhibition proportional to its concentration. D) The initial rate of defluorination, but not the ultimate extent, decreased in a PFAS-impacted groundwater matrix (Table S1). Error bars are smaller than the symbol sizes.

IAA sorption to SWy-3 was negligible (Figure S6). However, IAA sorption to ALA- and HDTMA-SWy-3 was significant. All the sorption isotherms were described using the Langmuir isotherm equation. The maximum sorption capacity (C_{max}) of IAA followed the order of SWy-3<HDTMA-SWy-3<ALA-SWy-3, i.e., 6, 140, and 168 mmol/kg, respectively (Table S3). The Langmuir constant, K_L, a measure of sorption affinity, followed the same trend.

There was little PFOS sorption to SWy-3, but there was a significant amount of PFOS sorption to ALA-SWy-3 (Figure S7). Interestingly, there appeared to be two separate sorption stages. The first stage occurred at a low Ce concentration and it could be described using the Langmuir isotherm equation. The second stage could not be fitted with this model and may be related to the formation of (semi)micelle. The maximum sorption of PFOS to ALA-SWy-3 in the second stage was much higher, reaching as high as 1600 mmol/kg compared to only 10 mmol/kg to SWy-3, suggesting that the intercalated ALA served as an effective adsorbent.

3.3. PFOS defluorination

PFOS defluorination, calculated as the percent of measured fluoride ion relative to the total amount of fluoride available in initial PFOS, was monitored (Fig. 1A). Without applied UV radiation, fluoride was not generated in various combinations of IAA, SWy-3, and ALA-SWy-3 (<0.5%, data not shown). With UV radiation, fluoride generation was less than 5% in water, IAA, SWy-3 or their combinations. In contrast, significant defluorination was observed in the presence of ALA-SWy-3, reaching 41%. At a higher clay concentration (5 g/L), the extent of defluorination reached as high as 71% (Fig. 1A). However, spiking of IAA at 0, 3 and 6 h did not increase fluoride yield, suggesting that hydrated electrons generated from excess IAA were not used to degrade PFOS. A likely reason may be that excess IAA could not enter the interlayer of montmorillonite because of a limited sorption capacity of the intercalated ALA, and thus hydrated electrons were likely generated outside the clay interlayer and would not have a chance to degrade the interlayer PFOS. .

The presence of bicarbonate and nitrate anions decreased both the initial rate and final extent of PFOS defluorination (Fig. 1B-C), with nitrate exhibiting a greater inhibitory effect. The extent of inhibition was proportional to the concentration of these competing anions. The presence of PFAS-impacted natural groundwater did not affect the rate and extent of defluorination (Fig. 1D), even in the presence of 3.1 mM chloride anion (Table S1). Some fluoride was generated without PFOS and ALA-SWy-3, likely due to direct photolysis of native PFASs in groundwater by UV light.

3.4. PFOS degradation

The extent of defluorination does not necessarily represent the extent of degradation, because intermediate transformation products may accumulate over time. Thus, liquid chromatography-high

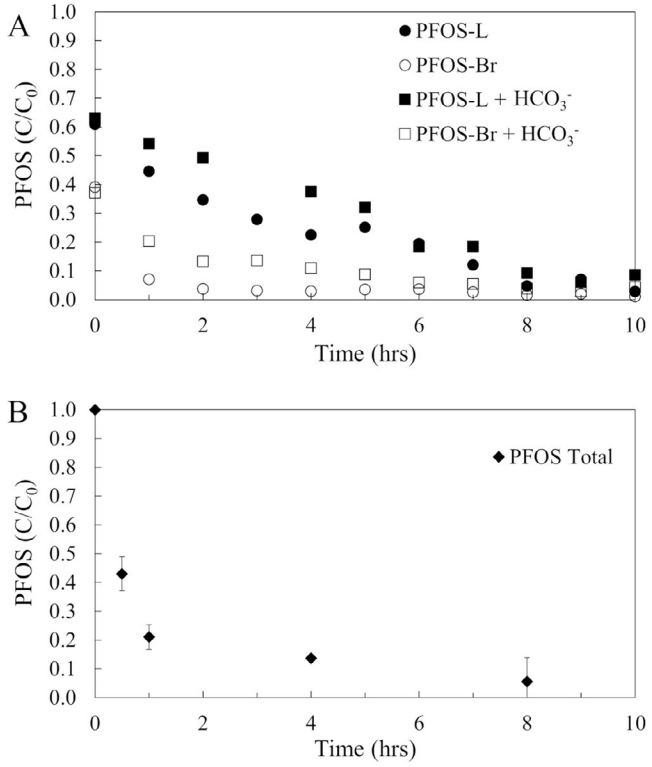

Fig. 2. Removal of PFOS over time. All PFOS starting concentrations were 10 ppm, all IAA concentrations were 1 mM, and all clay concentrations were 2.2 g/L. A) PFOS degradation shown as both branched and linear isomers in water and in 1 mM bicarbonate solution. Total PFOS removal was 97% by 10 h. B) PFOS degradation under the above conditions except that a higher concentration of ALA-SWy-3 (5 g/L) was used and IAA was added at 0, 3 and 6 h. PFOS removal reached approximately 95% in 8 h. Error bars are smaller than the symbol sizes.

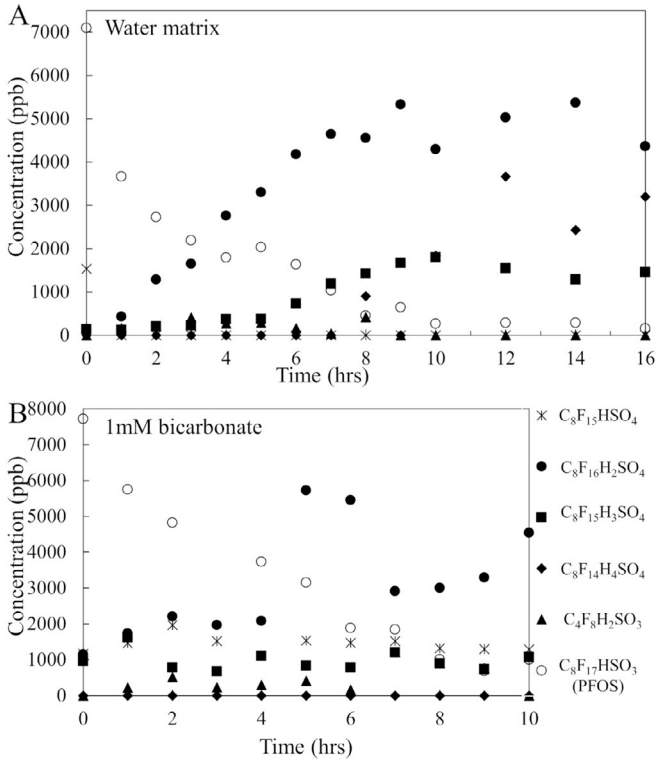

Fig. 3. Degradation of PFOS and production of intermediate products over time in a solution of 10 ppm PFOS, 1 mM IAA, and 2.2 g/L ALA-SWy-3. Concentrations are shown as percentages of the starting PFOS concentration, C_0. A) PFOS degradation in a water matrix; B) PFOS degradation in a matrix also containing 1 mM bicarbonate.

resolution mass spectrometric (LC–HRMS) analysis was performed to quantify PFOS and its transformation products. Interestingly, nearly all branched PFOS was removed in both water and bicarbonate solutions within two hours, but it took much longer to remove linear PFOS (Fig. 2A), consistent with a previous study (Jin and Zhang 2015). By 9 h, total PFOS concentration decreased by 90%. By 10 h, over 90% of the linear and nearly 100% of the branched PFOS were removed from solution. Consistent with the defluorination result (Fig. 1B), the presence of bicarbonate inhibited the removal rate of both linear and branched PFOS (Fig. 2A).

In the experiment with 5 g/L ALA-SWy-3 concentration (Fig. 2B), the concentration of total PFOS dropped quickly within the first half hour followed by a slower removal period. Rapid removal of PFOS (Fig. 2B) but little fluoride accumulation (Fig. 1A) in the first half hour suggests that degradation intermediates were formed, but over extended time, these products were degraded to generate fluoride (Fig. 1A). By approximately 5 h, PFOS was removed by 90%.

LC–HRMS analysis revealed that PFOS removal from aqueous solution was a result of sorption and degradation. The PFOS stock solution contained a small amount of $C_8F_{15}HSO_4$ (10–20%) and other minor impurities. Both PFOS and these impurities degraded over time. In 16 h, there was over 95% removal of PFOS and $C_8F_{15}HSO_4$. Correspondingly, three degradation products, $C_8F_{16}H_2SO_3$, $C_8F_{15}H_3SO_3$, and $C_8F_{14}H_4SO_3$ accumulated (Figs. 3& S8, and Table S4). There was a time lag between PFOS degradation and its first product formation, $C_8F_{16}H_2SO_3$, suggesting that removal of PFOS was initially due to sorption to ALA-SWy-3, but subsequently due to degradation. Minor amounts of $C_4F_8H_2SO_3$ and $C_8FH_{17}SO_3$ were also detected. In the presence of bicarbonate, there was no significant difference in the relative amounts of these degradation products. Interestingly, the impurity compound, $C_8F_{15}HSO_4$, was not degraded, suggesting that its degradation may be more difficult when bicarbonate was present. Other minor impurities including PFEtCHxS and PFNS were completely removed in 10 h, and the concentration of PFHpS was reduced by 50% (Figure S9).

3.5. Fluorine mass balance

The fluorine mass balance was calculated based on measured PFOS, impurities, and transformation products (Gu et al., 2020). The calculated values ranged from 50 to 95% (Figure S10), with a poor balance near the beginning and a much better one towards the end (~8 h). The lowest fluorine mass balance at 1 hour corresponded to the sorption maximum but before any significant degradation (Fig. 3A). Because the fluorine mass balance was calculated from aqueous concentrations of PFOS and all transformation products, PFOS sorption would result in an underestimate. At later time points, a nearly complete fluorine mass balance suggests that degradation was dominant, and any transformation products and fluoride did not sorb to ALA-SWy-3.

4. Discussion

4.1. Sorption of IAA and PFOS to SWy-3 and ALA-SWy-3

A considerably higher amount of IAA sorption to ALA-SWy-3 and HDTMA-SWy-3 than to SWy-3 (Figure S6) is likely due to the expanded interlayer spacing and the intercalated ALA/HDTMA, thus increasing the number of sorption sites (Solin, 1997). Likewise, the PFOS sorption capacity of ALA-SWy-3 reached up to 1600 mmol/kg (Figure S7), which is orders of magnitude higher

than PFAS sorption to soils (Milinovic et al., 2015) and mineral surfaces (Johnson et al., 2007; Wang et al., 2012; Wang and Shih 2011; Zhao et al., 2014). This level of PFOS sorption is in the range of those by custom resins (1000 to 5000 mmol/kg of substrate, depending on the resin type and pH) (Deng et al., 2010; Yu et al., 2009; Zaggia et al., 2016). However, many of these systems require non-circumneutral pH, and some even require pH values higher than 10, suggesting that adjustment of pH would be required before the wastewater could be discharged (Zhang et al., 2019). The high sorption capacities of both IAA and PFOS at neutral pH, as shown in this study, would facilitate degradation of PFOS at environmentally friendly pH.

4.2. Effects of co-present groundwater constituents

The greater amount of inhibition by nitrate than by bicarbonate (Fig. 1) was consistent with the result of a previous study (Gu et al., 2017a). A likely reason is that the reaction of hydrated electrons with nitrate is much faster than with PFOS, but the reaction of hydrated electrons with bicarbonate is slower (Buxton et al., 1988; Huang et al., 2007). Nonetheless, the inhibitory effect of bicarbonate was still present (Fig. 1B). In this case, competitive sorption is a likely reason, because the montmorillonite scaffold may not be fully efficient to block entry of anions such as nitrate and bicarbonate.

The PFOS degradation experiment showed that a high level of chloride (3.1 mM) in a groundwater matrix, along with some levels of nitrate (0.15 mM), sulfate (0.11 mM) and dissolved organic carbon (DOC, 0.574 mg/L), only decreased the rate of defluorination, not the final extent. In fact, the extent of impact was similar to that by 0.1 mM nitrate alone (Fig. 3). However, in natural groundwater, DOC concentration can range from 2 to 14 mg/L (Pabich et al., 2001; Striegl et al., 2005), and the effect of DOC may be more important, because it may serve as electron shuttle during solvated electron generation (Guo et al., 2019) and/or block PFOS sorption sites of ALA by competitive sorption.

4.3. Mechanisms of PFOS degradation by hydrated electrons

Combining the ALA intercalation, IAA and PFOS sorption, and subsequent degradation of PFOS, a schematic model can be proposed (Fig. 4): 1) ALA enters the interlayer region of montmorillonite, expanding the interlayer spacing and increasing surface area; 2) IAA and PFOS enter the expanded interlayer region and co-sorb to ALA; 3) Upon irradiation, IAA emits hydrated electrons and indole radical cations; 4) PFOS is degraded by hydrated electrons. Generation of hydrated electrons was confirmed previously, based on a combination of electron paramagnetic resonance (EPR) measurement, quenching test (DMPO), and Fourier transform infrared spectroscopy (Tian et al., 2016). Because the same source of hydrated electrons (IAA), UV lamp, and the experimental system were used in this study, it was certain that hydrated electrons were responsible for PFOS degradation.

This proposed model explains the enhanced sorption of IAA (Figure S6) and PFOS (Figure S7), and the enhanced rate and extent of PFOS degradation (Figs. 1& 2) by ALA-SWy-3 relative to SWy-3 alone. Instead of sorbing to SWy-3, IAA and PFOS sorb to ALA in the SWy-3 interlayer, which has a much higher sorption capacity. Furthermore, the co-localization of IAA and PFOS to the same polymer ALA decreases the path length that hydrated electrons must travel to the target PFOS molecule, thus enhancing its degradation and defluorination capacities.

Our observed time-course fluorine mass balance curve was different from those in photoreductive degradation of PFOS (Gu et al., 2020; Sun et al., 2018). In those photoreductive reaction systems, the fluorine mass balance decreased over reaction time, which was

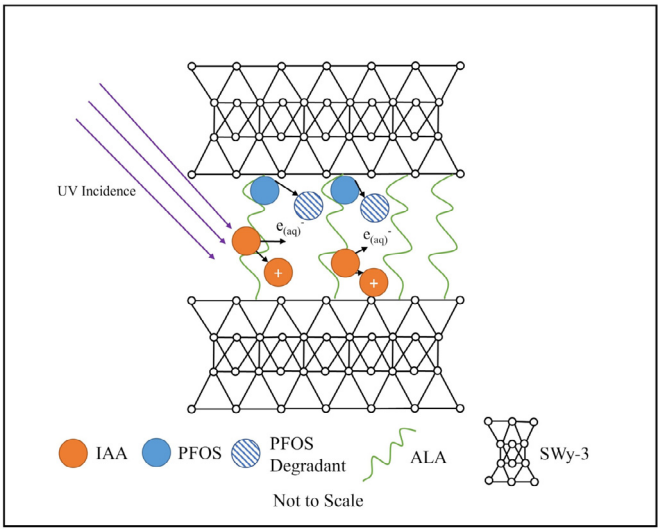

Fig. 4. A conceptual model showing the mechanism of PFOS degradation by hydrated electrons generated by UV irradiation of IAA. IAA and PFOS are co-sorbed to the organic polymer (ALA, HDTMA, or others), which is pre-inserted into the interlayer region of montmorillonite. For better viewing, the interlayer region is drawn not to scale.

ascribed to the formation of partially fluorinated intermediates. In our clay composite system, because IAA and PFOS were added nearly at the same time as UV irradiation, sorption and degradation should have been occurring simultaneously. At the beginning, PFOS sorption should be dominating over degradation, and thus the fluorine mass balance was low (Figure S10), because this balance calculation was based on total fluoride recovery in aqueous phase. However, with extended time, degradation became important, which explains the improved mass balance of fluorine. Towards the end of the degradation, all sorbed PFOS should have been degraded. The ~100% mass recovery of fluorine at the end of degradation experiment suggests that fluoride (Figure S5) and intermediate transformation products were fully recovered from aqueous phase and they were not sorbed to mineral surface, consistent with a previous study (Tian and Gu, 2018).

4.4. PFOS degradation pathways

PFAS degradation and defluorination are controlled by both the head group and the length of the fluoroalkyl chain (Cui et al., 2020), so it is specific to each class of PFASs. For sulfonated PFASs such as PFOS, there are three possible pathways of degradation: desulfonation, C–C breakage resulting in shorter chain compounds, and H/F exchange (Cui et al., 2020). The presence of sulfonated intermediate products (Fig. 3) suggests that even though the C-S bond has a lower energy (272 kJ/mol) than either the C–C bond (346 kJ/mol) or the C-F bond (485 kJ/mol), this C-S bond is not broken. Because the cleavage of C-S bond in PFOS by hydrated electrons has been observed in previous studies (Bentel et al., 2019; Gu et al., 2020; Gu et al., 2016; Gu et al., 2017a), lack of such cleavage in this study may be related to stabilization of the sulfonic head by the intercalated ALA, which is the likely site of adsorption (Zhang et al., 2011).

The detection of intermediate sulfonated transformation products, $C_8F_{16}H_2SO_3$, $C_8F_{15}H_3SO_3$, and $C_8F_{14}H_4SO_3$, suggests that hydrated electrons primarily break the C-F bonds to undergo H/F exchange. Although density functional theory calculation has shown that the two center C-F bonds have the lowest dissociation bond energy (Bentel et al., 2019), our products analyses do not support the C-F cleavage at the center position, suggesting that the degra-

dation kinetics of ALA-sorbed PFOS is different from homogeneous degradation reaction in aqueous solution. Furthermore, previous studies have shown stepwise defluorination (Bentel et al., 2019; Gu et al., 2020; Gu et al., 2016; Gu et al., 2017a; Qu et al., 2010; Song et al., 2013), but our time-course accumulation of intermediate transformation products suggest that there may be single and multiple H/F exchange reactions occurring at the same time. For example, the formation of $C_8F_{15}H_3SO_3$ was not at the expense of $C_8F_{16}H_2SO_3$. Likewise, the formation of $C_8F_{14}H_4SO_3$ was not at the expense of $C_8F_{15}H_3SO_3$ (Fig. 3). These data suggest that the second and third transformation products (and possibly other downstream products) may be formed from the parent PFOS directly, without sequentially going through the predecessor compounds. It has been suggested that it is less energetically taxing to further break down PFASs after they have undergone chain-shortening and that it may be more efficient to target the C–C bond initially as a means of energy conservation (Yang et al., 2013).

A measurable amount of $C_4F_8H_2SO_3$ indicates that there has been some chain-shortening, as the C–C bond has been broken in some of the PFOS molecules (Gu et al., 2016). Through molecular orbital calculation of PFOS, Gu et al. (2016) suggests that the lowest unoccupied molecular orbitals of PFOS is mainly located on the moiety of C4, C5, C6, C7, and C8 atoms, and external electron tends to localize in the region over these C atoms, thus weakening the C–C sigma bond and facilitating the C–C bond cleavage.

4.5. Energy requirements

In the 2.2 g/L nanocomposite experiment, it took approximately 9 h for one log unit (i.e., 90%) removal of PFOS (Fig. 2A) using a 36 W UV bulb in a 0.325 L reaction vessel, requiring almost 1000 w-h/L of energy. Alternatively, the higher clay concentration reactors reached a log unit removal of PFOS within 5 h (Fig. 2B). This reduced the power requirement almost by half, at 550 w-h/L. While this power requirement is not as efficient as electrochemical methods (Schaefer et al., 2019; Trautmann et al., 2015), it is about as efficient as other methods of hydrated electron generation, most notably the UV sulfite system (Gu et al., 2017a; Gu et al., 2017b).

To further optimize this system, the amount of organic polymer intercalated into the montmorillonite interlayer can be increased (Pagtalunan et al., 2018), which could increase sorption capacities of IAA and PFOS to further enhance PFOS degradation. Additionally, it is possible to increase the concentration of ALA-SWy-3 up to 10 or 15 g/L before there is a rheological change of SWy-3. This would further increase the rate and extent of PFOS degradation to optimize power generation.

4.6. Implications for treatment

This clay nanocomposite approach provides a remediation technology for PFASs using an easily made, robust, organo-modified clay, which does not require the application or use of hazardous chemicals. Because the ALA and montmorillonite bear minimal costs, approximately $90 and $2–5 per kg respectively, the predominant energy requirement is the operation of a UV lamp.

The observation that several impurities in the PFOS stock were also destroyed by this method suggest that this method would be viable against other recalcitrant PFASs. More importantly, the fact that this method worked in the presence of bicarbonate and nitrate, and even in natural groundwater matrix suggests this method may be broadly applicable to wastewater treatment. While the highest concentration of nitrate used in this study (1 mM) is far above the action limit set by the USEPA (Ward et al., 2018) and also above typical groundwater and surface freshwater levels (1–3 mg/L, which is 0.02 – 0.05 mM) (Spalding and Exner 1993), bicarbonate concentrations in natural groundwater can be as high as 500 mg/L (8.2 mM) in carbonate aquifers (Trainer and Heath 1976). Likewise, in PFAS-impacted groundwater, other PFASs may be at higher levels than those in the groundwater tested in this study (Guelfo and Adamson 2018; Houtz et al., 2013). Under these complex conditions, the degradation efficiency of PFASs may decrease. However, decreased efficiency may be compensated by increased loadings of ALA and ALA-SWy-3 nanocomposite. Additional research is required to fully demonstrate the utility of this method for scaling up. We envision that this method may be effective for treating concentrated PFASs in investigator-derived wastewater. In those cases, liters of concentrated PFAS wastewater may be treated using a larger UV lamp and larger benchtop reactors (5 – 25 liters), which increase both the volume of treatable liquid and the flux of the incident radiation. One potential drawback of this approach is buildup of degradation intermediates over the experimental time frame. However, with optimization (such as increased ALA loading) and prolonged reaction times, these intermediates may be further degraded. Alternatively, these intermediate products may be removed via either advanced oxidation processes or biological degradation.

5. Conclusions

These experimental results demonstrate that the degradation of PFOS via an IAA catalyzed reaction can be enhanced by organic modification of montmorillonite. The clay provides a protective scaffold for the organic polymer ALA, which can then function as a sorbent for PFASs. Upon exposure to hydrated electrons generated by the co-sorbed IAA under UV irradiation, PFOS undergoes degradation, forming intermediate products and fluoride. The presence of nitrate and bicarbonate inhibited PFOS degradation, with nitrate having a greater inhibition than bicarbonate. The technology provides the framework for an environmentally friendly and cost-effective technology, which does not require any use of any hazardous materials. Due to these reasons this technology provides the potential for an in-situ or ex-situ remediation technique for PFAS-concentrated, small-volume wastewater, such as investigator-derived wastewater However, additional research is needed to optimize the performance for scaling-up applications.

Author contributions

HD and CES conceived the research and guided the work; AK performed the research; CL and CG helped experimental setup and analysis of PFOS. DT and MS helped experimental setup and fluoride analysis. YJC and CPH helped intermediate daughter product analysis. All contributed to manuscript writing and revision.

Declaration of Competing Interest

The authors declare that they have no known competing financial interests or personal relationships that could have appeared to influence the work reported in this paper.

Acknowledgments

This research was supported by the Strategic Environmental Research and Development Program (ER-18–1526). We are grateful to five anonymous reviewers whose comments improved the quality of this manuscript.

Supplementary materials

Supplementary material associated with this article can be found, in the online version, at doi:10.1016/j.watres.2021.117221.

References

Bentel, M.J., Liu, Z., Yu, Y., Gao, J., Men, Y., Liu, J., 2020. Enhanced degradation of perfluorocarboxylic acids (PFCAs) by UV/sulfite treatment: reaction mechanisms and system efficiencies at pH 12. Environ. Sci. Technol. Lett. 7 (5), 351–357.

Bentel, M.J., Yu, Y., Xu, L., Li, Z., Wong, B.M., Men, Y., Liu, J., 2019. Defluorination of per- and polyfluoroalkyl substances (PFASs) with hydrated electrons: structural dependence and implications to PFAS remediation and management. Environ. Sci. Technol. 53 (7), 3718–3728.

Boyd, S.A., Mortland, M.M., Chiou, C.T., 1988. Sorption characteristics of organic–compounds on hexadecyltrimethylammonium-smectite. Soil Sci. Soc. Am. J. 52 (3), 652–657.

Brendel, S., Fetter, É., Staude, C., Vierke, L., Biegel-Engler, A., 2018. Short-chain perfluoroalkyl acids: environmental concerns and a regulatory strategy under REACH. Environ. Sci. Europe 30 (1), 9.

Buxton, G.V., Greenstock, C.L., Helman, W.P., Ross, A.B., 1988. Critical Review of rate constants for reactions of hydrated electrons, hydrogen atoms and hydroxyl radicals (·OH/·O− in Aqueous Solution. J. Phys. Chem. Ref. Data 17 (2), 513–886.

Chen, H., Kenny, J., 2007. A study of pH effects on humic substances using chemometric analysis of excitation-emission matrices. Ann. Environ. Sci. 1 (1–9).

Chen, Z., Li, C., Gao, J., Dong, H., Chen, Y., Wu, B., Gu, C., 2020. Efficient reductive destruction of perfluoroalkyl substances under self-assembled micelle confinement. Environ. Sci. Technol. 54 (8), 5178–5185.

Cheng, J., Vecitis, C.D., Park, H., Mader, B.T., Hoffmann, M.R., 2010. Sonochemical degradation of perfluorooctane sulfonate (PFOS) and perfluorooctanoate (PFOA) in groundwater: kinetic effects of matrix inorganics. Environ. Sci. Technol. 44 (1), 445–450.

Cooke, M.Emergency, O.o.L.a., 2017. Technical Fact Sheet – Perfluorooctane Sulfonate (PFOS) and Perfluorooctanoic Acid (PFOA). United States Envrionmental Protection Agency.

Cui, J., Gao, P., Deng, Y., 2020. Destruction of Per- and Polyfluoroalkyl Substances (PFAS) with advanced reduction processes (ARPs): a critical review. Environ. Sci. Technol. 54 (7), 3752–3766.

Deng, S., Yu, Q., Huang, J., Yu, G., 2010. Removal of perfluorooctane sulfonate from wastewater by anion exchange resins: effects of resin properties and solution chemistry. Water Res. 44 (18), 5188–5195.

Fernandez, N.A., Rodriguez-Freire, L., Keswani, M., Sierra-Alvarez, R., 2016. Effect of chemical structure on the sonochemical degradation of perfluoroalkyl and polyfluoroalkyl substances (PFASs). Environ. Sci. Water Res. Technol. 2 (6), 975–983.

Gu, P., Zhang, C., Sun, Z., Zhang, H., Zhou, Q., Lin, S., Rong, J., Hoffmann, M.R., 2020. Enhanced photoreductive degradation of perfluorooctanesulfonate by UV irradiation in the presence of ethylenediaminetetraacetic acid. Chem. Eng. J. 379, 122338.

Gu, Y., Dong, W., Luo, C., Liu, T., 2016. Efficient Reductive Decomposition of Perfluorooctanesulfonate in a High Photon Flux UV/Sulfite System. Environ. Sci. Technol. 50 (19), 10554–10561.

Gu, Y., Liu, T., Wang, H., Han, H., Dong, W., 2017a. Hydrated electron based decomposition of perfluorooctane sulfonate (PFOS) in the VUV/sulfite system. Sci. Total Environ. 607-608, 541–548.

Gu, Y., Liu, T., Zhang, Q., Dong, W., 2017b. Efficient decomposition of perfluorooctanoic acid by a high photon flux UV/sulfite process: kinetics and associated toxicity. Chem. Eng. J. 326, 1125–1133.

Guelfo, J.L., Adamson, D.T., 2018. Evaluation of a national data set for insights into sources, composition, and concentrations of per- and polyfluoroalkyl substances (PFASs) in U.S. drinking water. Environ. Pollut. 236, 505–513.

Guo, Chenxi, Zhang, Chaojie, Sun, Zhuyu, et al., 2019. Synergistic impact of humic acid on the photo-reductive decomposition of perfluorooctanoic acid. Chem. Eng. J. 360, 1101–1110.

Houtz, E.F., Higgins, C.P., Field, J.A., Sedlak, D.L., 2013. Persistence of Perfluoroalkyl Acid Precursors in AFFF-Impacted Groundwater and Soil. Environ. Sci. Technol. 47 (15), 8187–8195.

Huang, L., Dong, W., Hou, H., 2007. Investigation of the reactivity of hydrated electron toward perfluorinated carboxylates by laser flash photolysis. Chem. Phys. Lett. 436 (1), 124–128.

Javed, H., Lyu, C., Sun, R., Zhang, D., Alvarez, P.J.J, 2020. Discerning the inefficacy of hydroxyl radicals during perfluorooctanoic acid degradation. Chemosphere 247, 125883.

Jin, L., Zhang, P., 2015. Photochemical decomposition of perfluorooctane sulfonate (PFOS) in an anoxic alkaline solution by 185nm vacuum ultraviolet. Chem. Eng. J. 280, 241–247.

Johnson, R.L., Anschutz, A.J., Smolen, J.M., Simcik, M.F., Penn, R.L., 2007. The adsorption of perfluorooctane sulfonate onto sand, clay, and iron oxide surfaces. J. Chem. Eng. Data 52 (4), 1165–1170.

Kabadi, S.V., Fisher, J.W., Doerge, D.R., Mehta, D., Aungst, J., Rice, P., 2020. Characterizing biopersistence potential of the metabolite 5:3 fluorotelomer carboxylic acid after repeated oral exposure to the 6:2 fluorotelomer alcohol. Toxicol. Appl. Pharmacol. 388, 114878.

Lewis, A.J., Joyce, T., Hadaya, M., Ebrahimi, F., Dragiev, I., Giardetti, N., Yang, J., Fridman, G., Rabinovich, A., Fridman, A.A., McKenzie, E.R., Sales, C.M., 2020. Rapid degradation of PFAS in aqueous solutions by reverse vortex flow gliding arc plasma. Environ. Sci. Water Res. Technol. 6 (4), 1044–1057.

Liu, H., Yuan, P., Qin, Z., Liu, D., Tan, D., Zhu, J., He, H., 2013. Thermal degradation of organic matter in the interlayer clay–organic complex: a TG-FTIR study on a montmorillonite/12-aminolauric acid system. Appl. Clay Sci. 80-81, 398–406.

Marier, J.R., Rose, D, 1966. The fluoride Content of some foods and beverages–a brief survey using a modified Zr-SPADNS method. J. Food Sci. 31 (6), 941–946.

Milinovic, J., Lacorte, S., Vidal, M., Rigol, A., 2015. Sorption behaviour of perfluoroalkyl substances in soils. Sci. Total Environ. 511, 63–71.

Miura, A., Fukuchi, S., Okabe, R., Fukushima, M., Sasaki, M., Sato, T., 2011. Effect of different fractions of weathered pumice in the formation of humic-like substances. Clay Miner. 46 (4), 637–648.

O'Hagan, D., 2008. Understanding organofluorine chemistry. An introduction to the C–F bond. Chem. Soc. Rev. 37 (2), 308–319.

Oviedo, C., Rodríguez, J., 2003. EDTA: the chelating agent under environmental scrutiny. Química Nova 26, 901–905.

Pagtalunan, C.A.M., Sumera, F.C., Conato, M.T, 2018. Synthesis and characterization of 12-aminolauric acid-modified montmorillonite for catalytic application. AIP Conf. Proc. 1958 (1), 020021.

Qu, Y., Zhang, C.-J., Chen, P., Zhou, Q., Zhang, W.-X., 2014. Effect of initial solution pH on photo-induced reductive decomposition of perfluorooctanoic acid. Chemosphere 107, 218–223.

Qu, Y., Zhang, C.J., Li, F., Chen, J., Zhou, Q., 2010. Photo-reductive defluorination of perfluorooctanoic acid in water. Water Res. 44 (9), 2939–2947.

Pabich, W.J., Valiela, I., Hemond, H.F., 2001. Relationship between DOC concentration and vadose zone thickness and depth below water table in groundwater of Cape Cod. U.S.A. Biogeochem. 55 (3), 247–268.

Spalding, R.F., Exner, M.E., 1993. Occurrence of Nitrate in Groundwater—A Review. J. Environ. Qual. 22 (3), 392–402.

Rice, P.A., Aungst, J., Cooper, J., Bandele, O., Kabadi, S.V., 2020. Comparative analysis of the toxicological databases for 6:2 fluorotelomer alcohol (6:2 FTOH) and perfluorohexanoic acid (PFHxA). Food Chem. Toxicol. 138, 111210.

Schaefer, C.E., Andaya, C., Maizel, A., Higgins, C.P., 2019. Assessing continued electrochemical treatment of groundwater impacted by aqueous film-forming foams. J. Environ. Eng. 145 (12), 06019007.

Shoemaker, J., 2018. Method 537.1. Determination of Selected Perfluorinated Alkyl Acids in Drinking Water By Solid Phase Extraction and Liquid Chromatography/Tandem Mass Spectrometry (LC/MS/MS), pp. 1–50 Agency, U.S.E.P. (ed).

Solin, S.A., 1997. CLAYS AND CLAY INTERCALATION COMPOUNDS:properties and Physical Phenomena. Annu. Rev. Mater. Sci. 27 (1), 89–115.

Song, Z., Tang, H., Wang, N., Zhu, L., 2013. Reductive defluorination of perfluorooctanoic acid by hydrated electrons in a sulfite-mediated UV photochemical system. J. Hazard. Mater. 262, 332–338.

Striegl, R.G., Aiken, G.R., Dornblaser, M.M., Raymond, P.A., Wickland, K.P., 2005. A decrease in discharge-normalized DOC export by the Yukon River during summer through autumn. Geophys. Res. Lett. 32 (21), L21413. doi:10.1029/2005GL024413.

Sun, Z., Zhang, C., Xing, L., Zhou, Q., Dong, W., Hoffmann, M.R., 2018. UV/Nitrilotriacetic Acid Process as a Novel Strategy for Efficient Photoreductive Degradation of Perfluorooctanesulfonate. Environ. Sci. Technol. 52 (5), 2953–2962.

Sznajder-Katarzyńska, K., Surma, M., Cieślik, I., 2019. A review of perfluoroalkyl acids (PFAAs) in terms of sources, applications, human exposure, dietary intake, toxicity. Legal Regul. Methods Determ. 2019.

Tang, Y.W., Bonner, J., 1948. The enzymatic inactivation of indole acetic acid. II. The physiology of the enzyme. Am. J. Bot. 35 (9), 570–578.

Tian, H.T., Gao, J., Li, H., Boyd, S.A., Gu, C., 2016. Complete defluorination of perfluorinated compounds by hydrated electrons generated from 3-indole-acetic-acid in organomodified montmorillonite. Sci. Rep. 6, 32949.

Tian, H.T., Gu, C., 2018. Effects of different factors on photodefluorination of perfluorinated compounds by hydrated electrons in organo-montmorillonite system. Chemosphere 191, 280–287.

Trainer, F.W., Heath, R.C., 1976. Bicarbonate content of groundwater in carbonate rock in eastern North America. J. Hydrol. (Amst) 31 (1–2), 37–55.

Trautmann, A.M., Schell, H., Schmidt, K.R., Mangold, K.-M., Tiehm, A., 2015. Electrochemical degradation of perfluoroalkyl and polyfluoroalkyl substances (PFASs) in groundwater. Water Sci. Technol. 71 (10), 1569–1575.

Wang, F., Liu, C., Shih, K., 2012. Adsorption behavior of perfluorooctanesulfonate (PFOS) and perfluorooctanoate (PFOA) on boehmite. Chemosphere 89 (8), 1009–1014.

Wang, F., Shih, K., 2011. Adsorption of perfluorooctanesulfonate (PFOS) and perfluorooctanoate (PFOA) on alumina: influence of solution pH and cations. Water Res. 45 (9), 2925–2930.

Wang, Y., Pierce, R.D., Shi, H., Li, C., Huang, Q., 2020. Electrochemical degradation of perfluoroalkyl acids by titanium suboxide anodes. Environ. Sci. Water Res. Technol. 6 (1), 144–152.

Ward, M.H., Jones, R.R., Brender, J.D., de Kok, T.M., Weyer, P.J., Nolan, B.T., Villanueva, C.M., van Breda, S.G., 2018. Drinking water nitrate and human health: an updated review. Int. J. Environ. Res. Public Health 15 (7), 1557.

Wilding, M., Walsh, E.F.A., Dorrian, S.J., Scott, C, 2015. Identification of novel transaminases from a 12-aminododecanoic acid-metabolizing Pseudomonas strain. Microb. Biotechnol. 8 (4), 665–672.

Yang, S., Cheng, J., Sun, J., Hu, Y., Liang, X., 2013. Defluorination of aqueous perfluorooctanesulfonate by activated persulfate oxidation. PLoS ONE 8 (10), e74877.

Yu, Q., Zhang, R., Deng, S., Huang, J., Yu, G., 2009. Sorption of perfluorooctane sulfonate and perfluorooctanoate on activated carbons and resin: kinetic and isotherm study. Water Res. 43 (4), 1150–1158.

Zaggia, A., Conte, L., Falletti, L., Fant, M., Chiorboli, A., 2016. Use of strong anion exchange resins for the removal of perfluoroalkylated substances from contaminated drinking water in batch and continuous pilot plants. Water Res. 91, 137–146.

Zeng, Q., Dong, H., Zhao, L., Huang, Q., 2016. Preservation of organic matter in nontronite against iron redox cycling. Am. Mineral. 101 (1), 120–133.
Zhang, D.Q., Zhang, W.L., Liang, Y.N., 2019. Adsorption of perfluoroalkyl and polyfluoroalkyl substances (PFASs) from aqueous solution - A review. Sci. Total Environ. 694, 133606.
Zhang, Q., Deng, S., Yu, G., Huang, J., 2011. Removal of perfluorooctane sulfonate from aqueous solution by crosslinked chitosan beads: sorption kinetics and uptake mechanism. Bioresour. Technol. 102 (3), 2265–2271.
Zhao, L., Bian, J., Zhang, Y., Zhu, L., Liu, Z., 2014. Comparison of the sorption behaviors and mechanisms of perfluorosulfonates and perfluorocarboxylic acids on three kinds of clay minerals. Chemosphere 114, 51–58.